IAC-15,C2,5,3,x29660

STRUCTURAL HEALTH MONITORING DURING SUBORBITAL SPACE FLIGHT

Andrei Zagrai[1], [1]New Mexico Institute of Mining and Technology, USA, azagrai@nmt.edu

Nickolas Demidovich[2], Benjamin Cooper[1], Jon Schlavin[1], Chris White[1], and Seth S. Kessler[3], Joseph Macgillivray[1], Samuel Chesebrough[1], Erik Magnuson[1], Lloyd Puckett[1], Karen Tena[1], Jaclene Gutierrez[1], Blaine Trujillo[1], David Siler[1], Tiffany Gonzales[1]
[1]New Mexico Institute of Mining and Technology, 801 Leroy Pl., 124 Weir Hall, Socorro, NM 87801, USA.
[2]US Federal Aviation administration (FAA), [3]Metis Design Corporation, 205 Portland St, Boston, MA 02114, USA

Structural Health Monitoring (SHM) has potential to revolutionize assessment and qualification of space vehicles. This technology is seen as important element in improving safety of space travel and reducing spacecraft operation costs. It is envisioned that structural health monitoring will provide near real-time information on structural integrity and report potentially abnormal behaviour to astronauts or support personnel. In this capacity, SHM system is viewed as an integral part of spaceflight information system and flight recorder. A concept of spacecraft SHM system was implemented in a payload designed by New Mexico Institute of Mining and Technology and flown on NASA Flight Opportunity commercial suborbital spaceflight. The aim of the test was to investigate performance of state-of-the-art SHM technologies in launch, accent, space, and decent environments as well as survivability at landing. Two SHM approaches were considered: wireless strain and temperature sensing and active/passive embedded ultrasonic, which included elastic wave propagation studies, electro-mechanical impedance diagnostics, and acoustic emission monitoring. Wireless strain and temperature measurements, which university conducted in collaboration with Microstrain Corporation, allowed for collecting data at two locations inside payload and for investigating prospects of wireless sensing during commercial spaceflight. Interference with other payloads and vehicle's command/control/communication were considered and the test has demonstrated utility of on-board wireless sensing. The university cooperated with Metis Design Corporation on active and passive embedded ultrasonic experiments. Active ultrasonic testing provided data on variation of structural sound speed during the flight and confirmed noticeable difference for in-space and on-the ground conditions. Additional active ultrasonic experiments have demonstrated potential for in-flight detection of structural cracks and loose bolted joints. Acoustic emission activity was measured in the passive embedded ultrasonic experiment, which indicated possibility for sensing structural events. Collected structural health data indicates feasibility of SHM during suborbital flight and highlights importance of acquiring environmental parameters that could influence diagnostic decisions.

I. INTRODUCTION

Structural health monitoring (SHM) is aimed at providing near real-time information of structural integrity and reporting potentially abnormal behaviour. Space system SHM is unique and notably deviates from typical aircraft SHM applications because of its multi-functionality at various stages of the mission[1]. Research[2] has shown SHM utility in pre-launch diagnostics and qualification of the spacecraft. It may be used to monitor spacecraft structure during launch and provide benefits of in-orbit monitoring. Finally, it may record data on structural performance and potential damage during atmospheric re-entry of the spacecraft. This last application is critical for understanding of structural breakup during re-entry or re-certification of the landed spacecraft for the next mission.

Until recently, attention of the space community to SHM has been limited. The most likely reason for such an inattention is economics of space operation affecting opportunities (and needs) for non-destructive evaluation (NDE) during spaceflight. Previous work on pre-launch qualification[3], monitoring of thermal protection system and assessment of satellite bolted joints has influenced broader acceptance of SHM as an integral part of new generation of spacecrafts. Aiming to improve safety and reliability of commercial spacecrafts, SHM mission was extended from almost exclusively pre-launch diagnosis to structural condition monitoring during all stages of space flight. A significant step forward in addressing safety concerns was development of a flight information recorder, aka "black box". Initial configuration for such a recorder has been developed and tested by the Aerospace Corporation[4]. In the conducted tests[5], REBR has recorded accelerations, internal pressure and heat shield temperatures. However, to improve understanding of the break-up process or re-certification of reusable parts, it is important to record information on structural

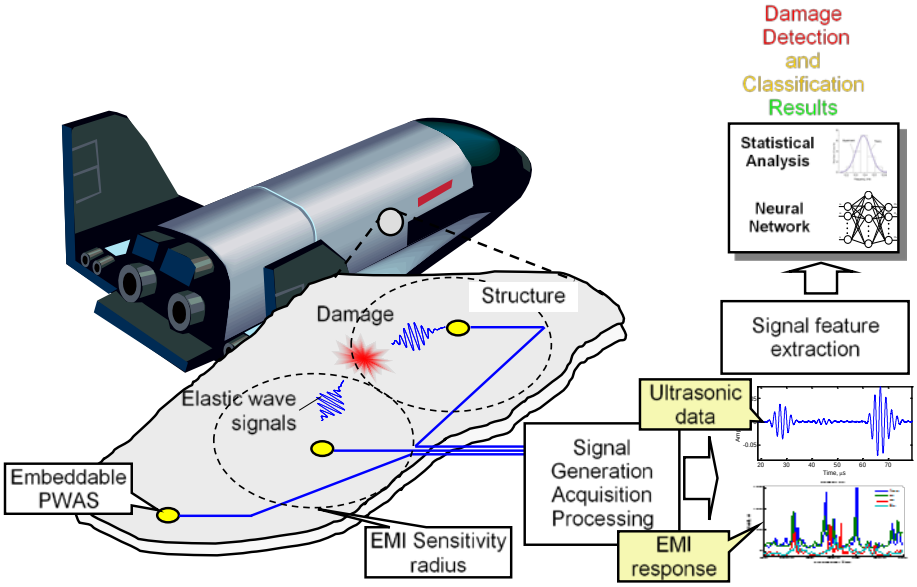

Fig. 1: A concept of SHM system for spacecraft utilizing piezoelectric wafer active sensors (PWAS) as transducers.

integrity. A number of approaches[6,7,8] have been suggested to perform this task, most of which were demonstrated either in laboratory or field (actual spacecraft load) testing. To investigate influence of environmental conditions on embedded ultrasonic testing, acoustic emission monitoring and wireless strain/temperature measurements, a stratospheric balloon test was conducted[9]. The tests demonstrated possibility of real-time ultrasonic measurements during flight and opened a way for technology integration into the sub-orbital vehicle. The payload containing a number of SHM experiments has been successfully flown on a sub-orbital spaceflight and results of this experiment are presented below.

II. TECHNOLOGY DESCRIPTION

A concept of the active SHM system of a spacecraft is depicted in Fig. 1. Small piezoelectric sensors may be attached or embedded into the spacecraft structure to enable passive and active detection of structural damage. Examples of passive assessment include monitoring of the acoustic emission activity, strain measurements, and impact detection. Information from such an assessment is typically very limited and does not offer sufficient details to estimate damage severity and criticality. For this reason, in addition to passive monitoring, active approach may be used to provide such details. Fig. 1 illustrates that embedded structural sensors transmit and receive elastic waves that are recoded and analysed by a processing unit. Frequency domain data enables electro-mechanical impedance assessment while time domain data furnish ultrasonically-derived characteristics and location of damage. Features sensitive to damage are derived from impedance and ultrasonic signatures and then are classified into three (healthy, moderate, unhealthy) states using statistical analysis or neural networks. This diagnostic decision is stored on board and may be also downlinked to a designated spacecraft control and monitoring station.

For structures with bonded or embedded piezoelectric wafer active sensors (PWAS), expansion and contraction of the sensor under applied continuous wave (CW) excitation result in associated dynamic axial forces and bending moments acting in the structure, Fig. 2a. This reaction opposing the sensor can be measured using a variety of circuits as frequency dependent impedance function[10]. One of the most reliable and accurate

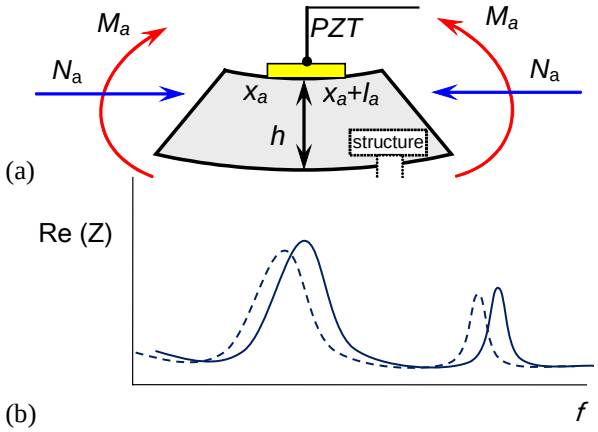

Fig. 2: Illustration of electro-mechanical impedance (EMI) method: (a) structural forces and moments created due to oscillations of the piezoelectric sensor, (b) Real part of impedance of intact (solid line) and damaged (dashed line) structures.

circuits is implemented in the HP (Agilent) line of impedance analysers. Mechanical to electrical (and vice versa) conversion in the piezoelectric material allow for manifestation of the structural dynamic response in the PWAS electrical signature[11],[12]. If damage (crack, fatigue, loose bolt) appear in the near field of the sensor, local structural response will change amplitudes and frequencies as indicated in Fig. 2b. Initial work on the electro-mechanical impedance method[13] highlighted opportunity to analyse structural dynamics through the sensor impedance signature. Mathematical description of the method may be seen in the expression below containing both structural, $Z_{str}(\omega)$, and sensor, $Z_{PZT}(\omega)$, impedance[14].

$$Z(\omega) = \left[i\omega C \left(1 - \kappa_{31}^2 \frac{Z_{str}(\omega)}{Z_{str}(\omega) + Z_{PZT}(\omega)} \right) \right]^{-1} \quad [1]$$

where ω is excitation frequency (rad/s), κ_{31} is electro-mechanical coupling coefficient for on-plane vibration, and C denotes the zero-load capacitance of the sensor. Because of participation of structural impedance in the total impedance measured at PWAS terminals, structural changes inflicted by damage will be reflected in $Z(\omega)$ and can be used for structural health monitoring.

To assess structural integrity far away from the sensor, an elastic wave approach is utilized. It encompasses an ultrasonic technology in which amplitude/phase of the transmitted wave changes as it propagates through damage[15]. Under applied transient excitation (blue curve in Fig. 3a), PWAS produces an ultrasonic pulse traveling through the structure and received by another sensor located some distance away from the excitation point, Fig. 1. The received signal, such as one depicted in Fig. 3a as a green line, contains structural characteristics associated with a particular structural state. Fig. 3b illustrates that differences in structural condition may cause signal amplitude changes, phase delays and nonlinear characteristics. By tracking these differences with respect to a baseline signal corresponding to healthy condition, one may assess structural damage such as cracks, loose bolts, delaminations, etc[16].

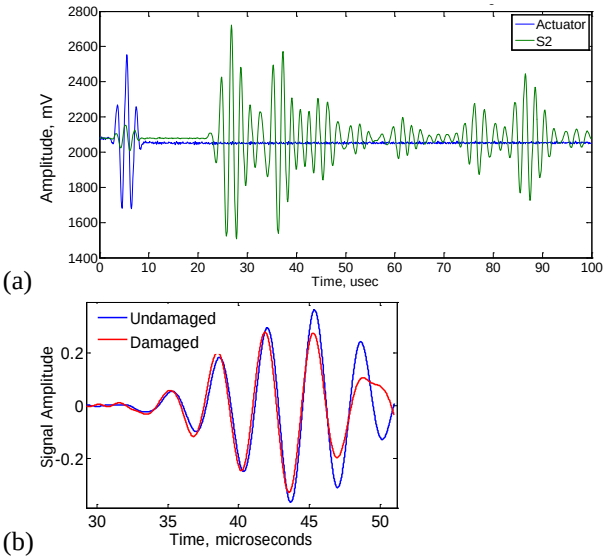

Fig. 3: (a) transmitted and received ultrasonic signals, (b) ultrasonic response of undamaged and damaged scenarios.

To test performance of wireless technology during suborbital flight, we decided to supplement SHM data with strain and temperature monitoring enabled by distributed wireless sensors. Wireless sensing is rather well established technology and does not require a detailed description of the measurement method.

II. FLIGHT MISSION AND PROFILE

The flight mission of New Mexico Tech payload was to test several SHM methodologies, SHM sensors and off-the-shelf SHM hardware in suborbital flight environment. Under the NASA Flight Opportunity Program (FOP), the payload designated as 38SB flew from Space Port America (New Mexico) on SL-8 flight. The UpAerospace's SpaceLoft rocket took off at 9:15 am; it landed 751.3 seconds (12.5 minutes) later, reaching maximum altitude of 117073.68 meters. Trajectory of the SL8 flight is presented in Fig. 4.

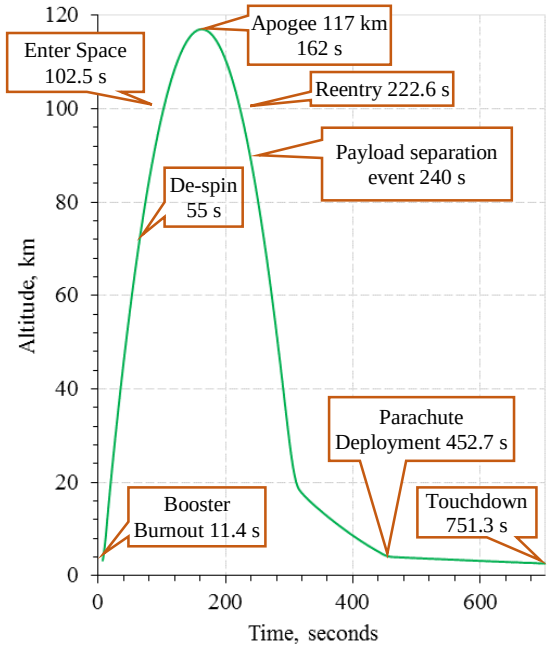

Fig. 4: Trajectory of SL-8 flight.

The payload carried to space a number of experiments aimed at demonstrating structural health monitoring during spaceflight. The mission was successful and New Mexico Tech team acquired valuable data for each experiment in a payload. Wireless sensors collected strain and temperature data, electromechanical impedance test investigated performance of piezoelectric sensors during suborbital flight, and structural sound speed was measured for the first time in space using unobtrusive embedded ultrasonic sensors. These sensors we also utilized to measure integrity of the payload and acoustic emission during all stages of the spaceflight from launch to landing.

II. PAYLOAD DESIGN

The payload design was governed by PTS10 payload configuration of UPAerospace's SpaceLoft rocket and consists of a cylindrical layered system of five aluminum plate as illustrated in Fig. 5. Bulk experimental modules and batteries to power them were located on the top and bottom plates separating payloads in the rocket. Two internal thin aluminum 6061-T6 plates were used in ultrasonic experiments and one thicker plate (1/8") carried experimental hardware. Diameter of the plates was 24.2 cm. The five plates were held together with six 25.4 cm (10") long all-thread rods. Position of each plate in the payload system can be adjusted using twelve 1/4" nuts.

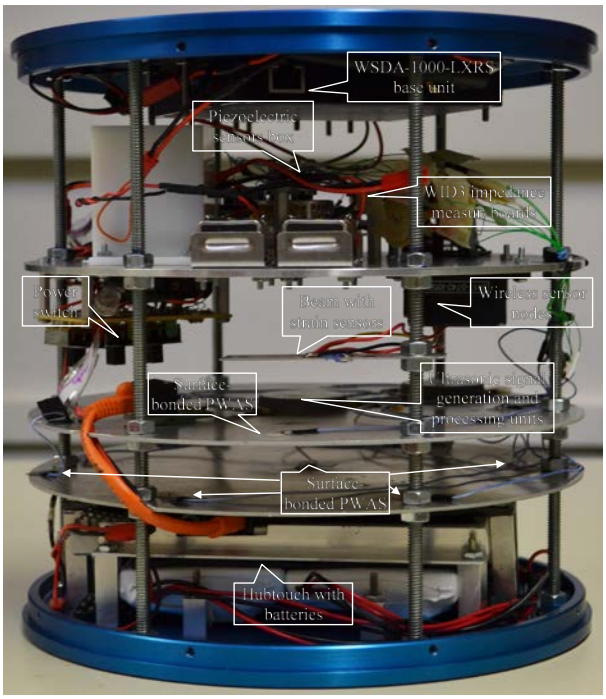

Fig. 5: 38SB payload carrying several SHM experiments.

Visible in Fig. 5, the bottom plate holds the Metis Hubtouch and its battery pack. Foam isolation was used between the Hubtouch and mounts to protect electronics from mechanical shocks. An orange cable connects Hubtouch with low profile ultrasonic signal generation and processing unit enabling elastic wave propagating experiment on the third plate. The top plate holds the Microstrain WSDA-1000-LXRS base unit and the battery used to power it. The plate below this (4th plate from bottom) holds two WID3 electro-mechanical impedance boards and the piezoelectric sensor experiment. On this plate, there are also the system power switch, two wireless sensor nodes, a 9V battery, and AAA battery pack for WID3. Power switch, wireless sensors nodes and a GoPro® camera are positioned on the back side of the plate. The camera (not pictured in Fig. 5) was installed underneath plate 4, above the beam with strain sensors.

The payload electrical design included a triggering system to power each sub-system and provide the user with visual feedback of the system status (off or on). A switch positioned underneath the 4th plate is distinguishable with three red LEDs signifying power delivery to a particular sub-systems. Each sub-system was turned on by engaging the switch about 1 hour before launch, which initiated data collection for wave propagation experiment and wireless sensing. An exception was the electro-mechanical impedance experiment, which was triggered by an accelerometer at the time of launch. 9V batteries positioned on the 4th plate powered switch and electro-mechanical impedance triggering circuit. Two additional units containing AAA batteries were placed under WID3 to power impedance measurement hardware. Total mass of the payload with all hardware was estimates close to 7 kg.

The payload configuration described above, allowed for implementing a number of experiments investigating possibility of real-time SHM during suborbital flight:

1. Wireless strain and temperature sensing in two locations inside payload.
2. Electro-mechanical impedance measurements enabling investigation of
    a. Piezoelectric sensor performance during suborbital flight
    b. Structural dynamic measurements of the 2nd plate
    c. Electro-mechanical impedance assessment of integrity of bolted joints.
3. Elastic wave propagation experiment consisting of :
    a. Structural (aluminum plate) sound speed measurements
    b. Detection of simulated crack
    c. Condition assessment of bolted joints
4. Acoustic emission monitoring.

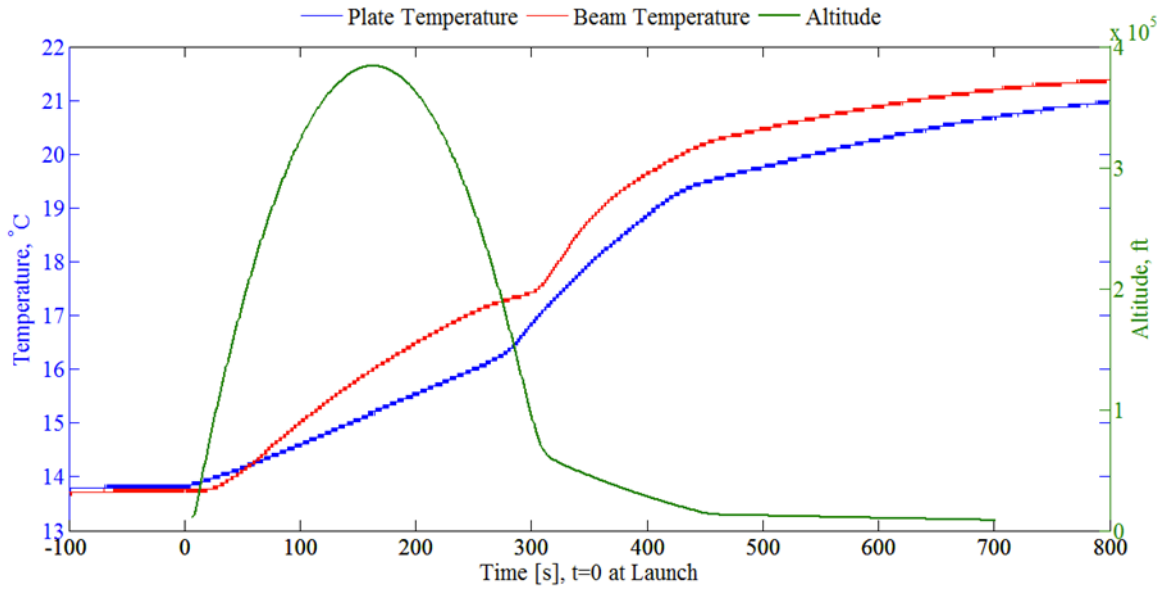

Fig. 6: Temperature inside S38 Payload collected wirelessly during SL8 mission..

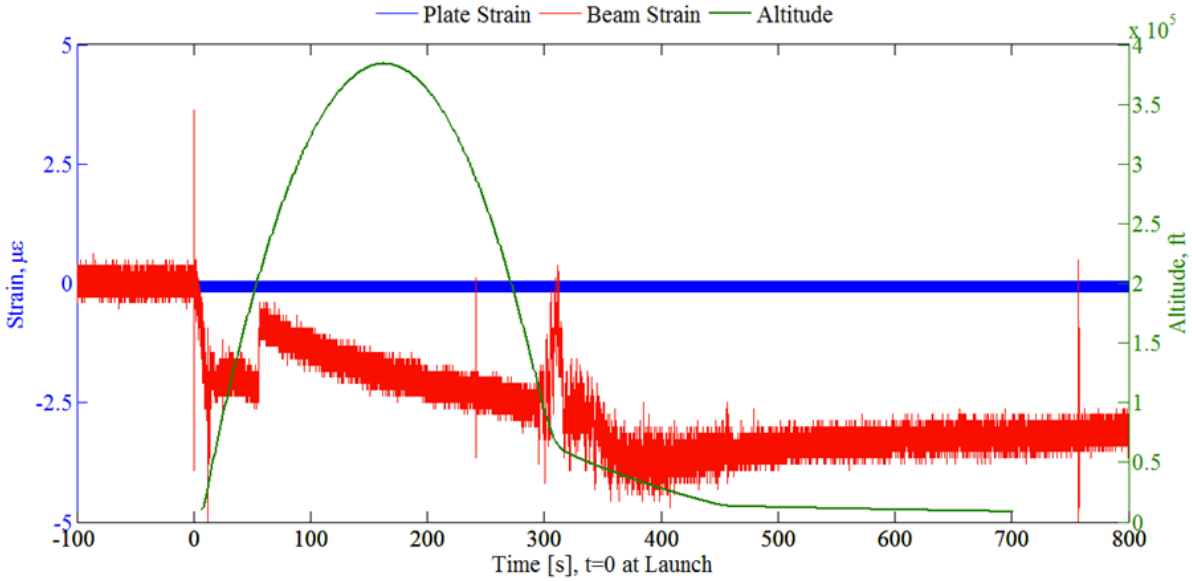

Fig. 7: Strain on two elements of S38 Payload collected wirelessly during SL8 mission.

II. SUBORBITAL FLIGHT SHM EXPERIMENTS

During the suborbital spaceflight, four SHM experiments listed above were conducted. The university collaborated with Metis Design Corporation on active and passive embedded ultrasonic experiments and with LORD Microstrain Corporation on wireless acquisition of strain and temperature data. Electro-mechanical impedance testing was implemented with measurement boards[17] provided by Los Alamos National Laboratory's Engineering Institute. Unfortunately, the electro-mechanical impedance boards malfunctioned during flight and no useful impedance data were collected. The other failure was GoPro® camera, which drained its batteries during launch delay of several hours.

II.I Wireless Strain and Temperature Sensing

Wireless strain and temperature measurements were aimed at investigating possibility of wireless communication and data acquisition during suborbital flight. Unfortunately, our team was not able to place any wireless nodes inside the rocket at locations outside the assigned PTS10 payload. For this reason separation between wireless nodes and a receiving WSDA1000

station was only 6 cm. Two wireless nodes were located on the other side of thick aluminum plate. Good wireless reception was achieved during the suborbital flight and data were collected successfully.

Strains were measured in two locations: on a cantilever beam (center of Fig. 5), and on a thick (1/8“) circular aluminum plate. In both cases, conventional foil strain gauges in full bridge configuration were utilized. A standard procedure for installation of foil strain gauges was followed, in which sensors were installed using space-qualified Hysol EA 9390 adhesive. Two wireless nodes were placed some distance from strain sensors on the backside of a thick aluminum plate. Temperature sensors were located inside wireless nodes and hence their location does not collocate with strain sensors. Wireless nodes were installed in the proximity of a technological window (there circular holes of less than 1 inch diameter) to space. This installation resulted in a configuration in which one node was in an immediate proximity to a window and the second node was located further away towards center of the payload.

Fig. 6 illustrates temperature data collected during suborbital flight and flight trajectory superimposed on temperature data. It should be noted that the wireless node connected to beam experiment (red curve) is located closer to the opening of the payload and is likely more affected by space environment. It is seen that temperature recorded by this node is higher (except at the beginning) than temperatures of the second node (blue curve) located further away from the opening. The second observation is three distinct segments of temperature deviation: the first segment is before beginning of flight on a launchpad, second segment is during active stage of the flight where temperature increases, the third segment occurs after atmosphere re-entry and parachute deployment that decelerated the rocket. The indicated three temperature segments correspond well with stages of the suborbital flight as seen in the trajectory plot.

Strain histories recorded during suborbital flight are presented in Fig. 7. Foil strain gauges were put in two locations: on the cantilever been attached to one of threaded pillars and on a circular plate supporting experimental hardware. As it could be seem in the figure, strain in the plate is constant with insignificant deviation, likely due to temperature increase during flight. Cantilever beam is much more compliant than a plate and shows the strain dependence reflecting dynamic events of the space vehicle. In particular, motor burnout, de-spin, payload separation, parachute release and landing are seen in the strain history. Strain measured on a fixed-free beam in the payload correlates well with dynamics of the payload.

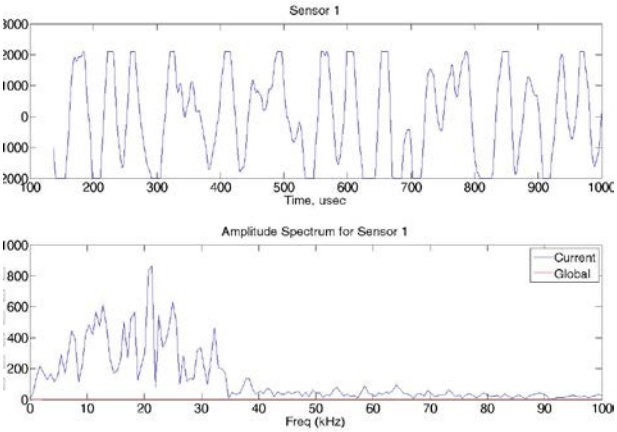

Fig. 8: Acoustic emission signal (top) and its spectrum (bottom) during booster burnout stage of the flight.

II.II Acoustic Emission Monitoring

Acoustic emissions during flight were recorded with the ultrasonic hardware operating in a passive mode. Passive mode was invoked between active scans, each of which lasted slightly more than 2 minutes (there were about 7 active scans for a duration of flight). For every active scan, two passive records were made. The record duration in the passive mode was 1 millisecond. Acoustic emission was measured with 6 sensors for several hours prior to and after the flight. There were 350 records of acoustic emission data, and a few events of the flight appear to have been captured. For example, Fig. 8 illustrated highly saturated signal measured at the liftoff. Spectral characteristic of this signal superimposed on top of an average global spectrum show substantial activity at low frequencies. It is believed that such a high-energy event is related to the initial booster burnout stage of the flight.

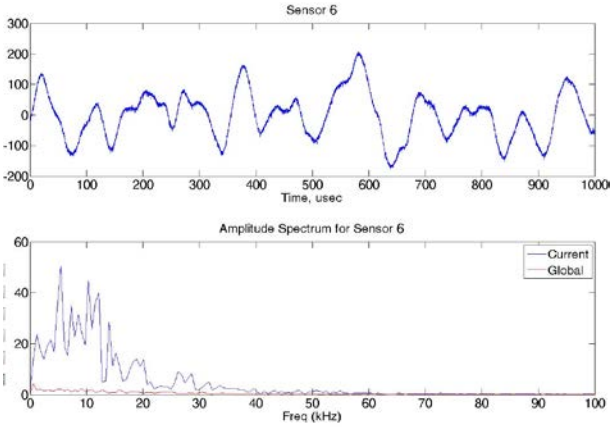

Fig. 9: Acoustic emission signal (top) and its spectrum (bottom) during payload separation event.

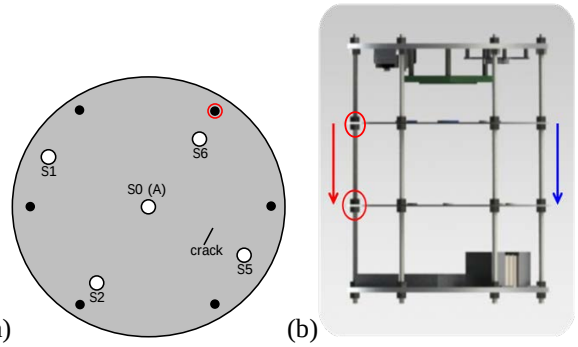

(a) (b)

Fig. 10: Scematics of wave propagation experiments: (a) a third circular plate with indicated sensors and simulated crack layout, (b) wave propagation paths for loose (red) and tight (blue) bolted joints.

The second interesting acoustic emission event occurred around 3 to 4 minutes after liftoff. This time approximately corresponds to the payload separation event. Hence it is suggested that this acoustic emission data corresponds to payload separation. One may note a difference between spectrum of this event (Fig. 9) and spectrum of the burnout stage (Fig. 8), which show much higher amplitude. Also noticeable in Fig. 9 is global spectrum of acoustic emission activity. Acoustic emission activity at higher frequencies were difficult to distinguish from background noise due to specifics of the hardware used to measure acoustic emission. It is suggested that in future flights, special acoustic emission hardware is used.

II.III Elastic Wave Propagation Experiments

Elastic wave propagation experiments utilized active mode of operation of ultrasonic equipment, which generated a pulse (blue curve in Fig. 3a) propagating from actuator S0 to sensors S1,S2,S5,S6 (Fig. 10a) and through threaded rods, Fig. 10b, to sensors S3 (under S2) and S5 (under S6) on the second plate. The second plate was identical to the third one (pictured in Fig. 10a) but with only two sensors S3 and S5 installed. Ultrasonic hardware on the third plate is depicted in Fig. 11. The active mode swept through frequencies of 50 kHz to 500 kHz in increments of 50 kHz. The entire cycle of active scan and two passive records took 140 seconds (2.3 minutes).

Structural sound speed measurements.

The active mode resulted in the 176 scans during the flight process, which included pre-launch, launch, flight, landing and recovery. Out of this family of records, 7 scans represented actual rocket flight. Ultrasonic signatures collected during flight were similar to a green curve presented in Fig. 3a. However, characteristics of signals were changing slightly depending on the stage of the flight. Fig. 12 presents details of elastic wave signals

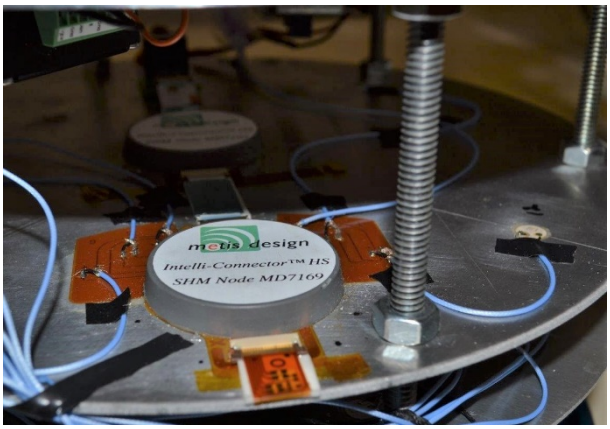

Fig. 11: Ultrasonic hardware installed on the third plate. Signal conditioning and processing unit is located close to the edge of the plate. A signal generation unit is visible at the center of the plate. Blue cables connect sensors and the signal conditioning unit.

collected with one of sensors at a fixed frequency over different stages of the flight. Signal records reveal that from Ground to Ascent and Apogee, the waveform generally shifts to the right, although the really pronounced shift is from Ground to Ascent. At some point in the Descent phase, the waveform has shift the furthest. Upon landing, the waveform has begun to shift back to the left, but after an hour of resting on the ground, the waveform would not returned completely to the previous Ground waveform position. Because some signal changes were observed after landing, it was proposed that the phenomenon of the phase shift may be attributed to structural temperature changes during flight. However, the permanent shift was still noticeable for hours indicating considerable influence of the flight on the structural assembly.

Besides the flight data collected, the elastic wave experiment was run in the same configuration several times before and after the space launch in a laboratory setting. Fig. 13 captures waveforms at 500 kHz recorded one hour before and one hour after the flight.

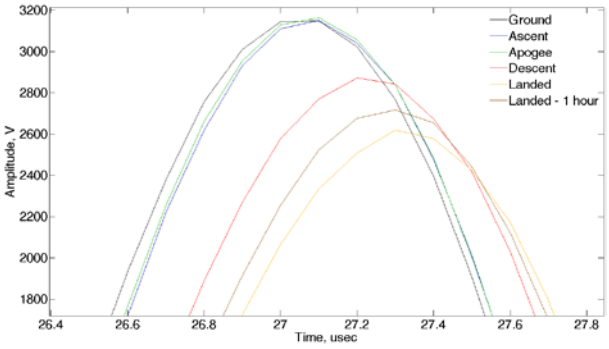

Fig. 12: Details of the ultrasonic signals showing differences for each stage of the suborbital flight.

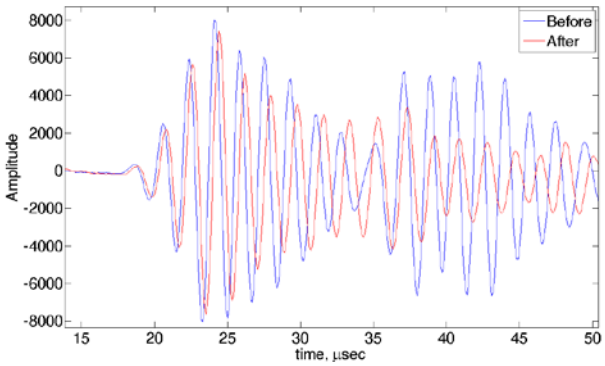

Fig. 13: Elastic wave signals collected one hour before and one hour after the flight at the highest excitation frequency of 500 kHz.

Differences in amplitude, phase and signal shape are noticeable. It was observed that the indicated differences were more pronounced at higher frequencies (e.g. 500 kHz) than at lower frequencies (e.g. 50 kHz).

To investigate a hypothesis of a substantial temperature contribution to variation of elastic wave signatures during suborbital flight, temperature data from a sensor inside the ultrasonic hardware unit were considered. It should be mentioned that temperatures recorded by this sensor are influenced by neighbouring electronics and do not reflect ambient temperatures. These temperature records, however, allow for studying temperature trend during suborbital flight.

Fig. 14 illustrates temperatures measured by a sensor inside the wave propagation hardware unit over the entire 400 minutes of data acquisition. Four data points are highlighted on the plot corresponding to launch, apogee, payload separation and touchdown of the space vehicle.

The internal node temperature rises throughout the flight to a peak of 59 ºC, and begins to cool off after touching down on the ground. It is also possible to see the rate of heating drop at the top of the temperature

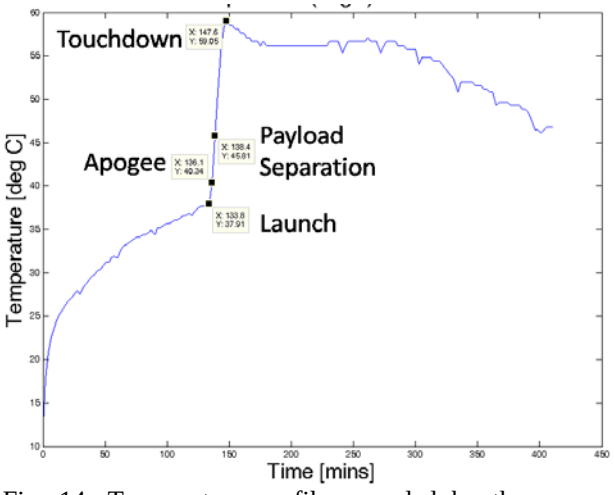

Fig. 14: Temperature profile recorded by the sensor inside the wave propagation hardware unit.

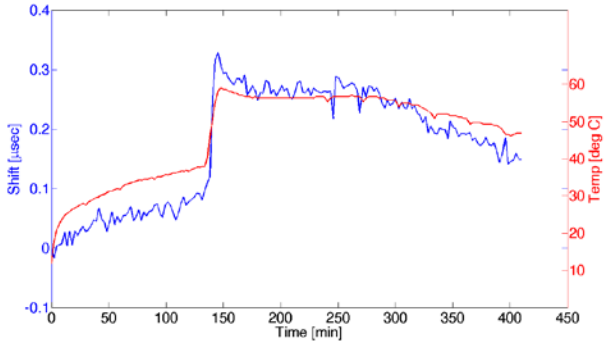

Fig. 15: Phase shift of the initial pulse of elastic waveform vs. temperature. Analysis was done for the signal collected by sensor S1 due to 500kHz excitation pulse applied to S0.

profile in Fig. 14 as a decrease in slope near the Touchdown label. To appreciate the relationship between the phase shift and temperature (as recorded during the space flight), the phase shift of the initial pulse was tracked through the full data collection period and a trend is presented in Fig. 15. As it is evident from the figure, the phase shift closely follows the temperature profile, which support previously presented observations.

The pre-flight Spaceport tests report a steady state temperature around 36 ºC and the post-flight New Mexico Tech runs report a steady state temperature around 39 ºC. Although the 3 degree difference between pre and post flight laboratory tests does not seem dramatic, any temperature difference should be removed to reduce the uncertainty in data analysis and interpretation. Between the two indicated laboratory data acquisitions, runs were found that were recorded at the same temperature. The data sets from these runs were processed and plotted against each other in Fig. 16. With the temperature-matched waveforms, one observes very little amplitude deviation and practically no phase shift in the measured elastic wave signals. This would suggest absence of a permanent effect of space environment (other than temperature) on the elastic wave measurements. However, another

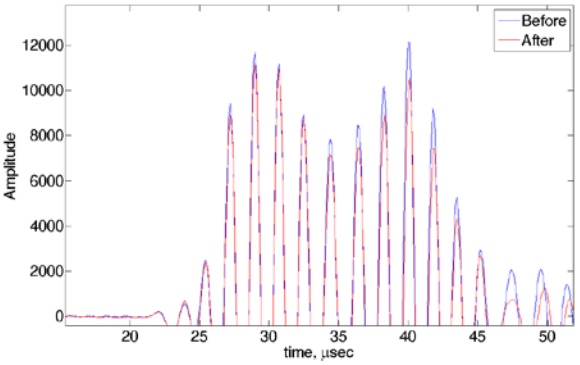

Fig. 16: Pre-flight (Launchpad, Spaceport America, NM, USA) and post-flight (NMT lab) test waveforms acquired at the same temperature.

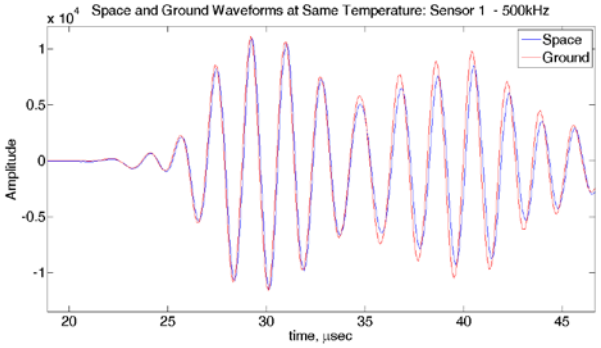

Fig. 17: Ultrasonic waveforms captured during spaceflight and on the ground at the same temperature of 50.79 degrees Celsius.

important aspect includes influence of space environment during suborbital flight, i.e. ultrasonic measurements at each segment of spaceship's trajectory.

During the cooling period on the ground, measurements were made at the same temperatures the payload experienced during flight. Using this data, it was possible to find records of ground measurements conducted at the same temperature as inflight tests. Comparison of signal obtained in-flight and on the ground at the same temperature of 50.79 ^{o}C is presented in Fig. 17. Interestingly there is no perfect overlay between two records. While differences for the first segment of the waveform are small, amplitude and phase changes are noticeable in the latter half of the elastic wave record. Our calculations suggest that the first pulse matches the faster symmetric elastic wave propagation mode (S0 mode), and the second pulse is the antisymmetric mode (A0). Comparison of the waveforms in Fig. 17 suggests that space environment very little affect the symmetric S0 wave propagation mode and noticeably affect the antisymmetric A0 wave propagation mode. Although the reason for the A0 variation during spaceflight awaits explanation, this effect should be accounted for while analysing structural health monitoring data and arriving at diagnostic decisions.

Condition assessment of bolted joints

Space structures almost always contain bolted joints. Ability to monitor integrity of the bolted joints is critical to the spacecraft SHM system. To study response of "loose", i.e. damaged, and "tight", i.e. healthy, bolted joints during suborbital flight, elastic waves transmitted by actuator S0 and received on the second plate (after propagating through threaded rods with nuts) by S5 and S3 were considered. The "loose" condition in this study was imitated by hand tightening nuts labelled in Fig. 10b.

The waveforms passing through both healthy and damaged bolted joints were recorded periodically throughout the flight and an example of signals corresponding to each segment of the flight is presented in Fig. 18. Comparison of top and bottom figures reveals obvious differences between the tight and loose conditions of the bolted pillars. The tight bolt case has a strongly visible wave pulse at 40-80 microseconds while the loose bolt case has a pulse with greatly reduced amplitude buried in noise. Apparently, the tightness of the bolt results in more stable connection of structural elements and allows for a better transmission of elastic energy through the bolted joint.

Although notable differences were observed between waveforms associated with tight and loose conditions of the bolted joint, wave forms within each of these groups (tight or loose) deviated only slightly during the flight stages. This is a valuable observation for practical implementation of SHM, since only minimal modifications to the damage classification scheme will need to be made for various stages of a flight. The largest deviations were seen in the descent stage. Discussion in the previous section of the paper suggests that these deviations are dominated by temperature-related effects during suborbital flight.

Detection of simulated crack

Fatigue cracks is of limited concern to expendable space vehicles, but they do pose a risk to reusable space vehicles. In this study, a crack was imitated by a 17×2 mm cut through the third plate. The cut is perpendicular to elastic wave propagation path as illustrated in Fig. 10a. Elastic waves were transmitted by actuator S0 and collected by sensors S1 and S5 located on healthy (intact material) and damaged (crack) wave propagation paths.

The signals from the sensors monitoring the crack were evaluated at various stages in the flight to explore deviations of elastic wave signals and determine if a crack can appropriately be detected at all times.

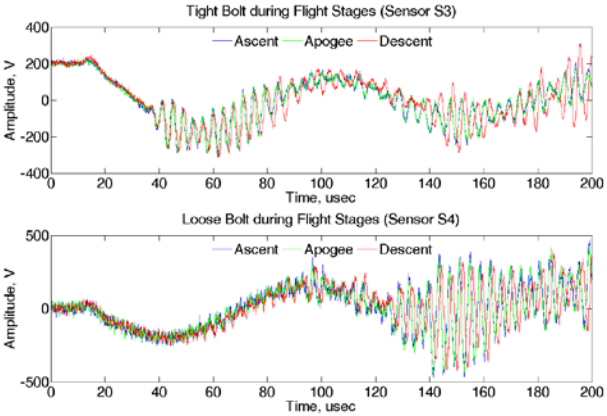

Fig. 18: (Top) ultrasonic signals propagated through healthy (tight) bolted joint. (Bottom) ultrasonic signals propagated through damaged (loose) bolted joint. Signals are presented for three stages of suborbital flight.

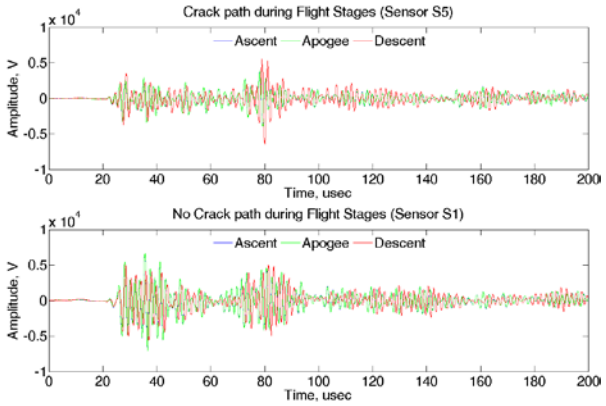

Fig. 19: (Top) ultrasonic signals propagated through healthy (no crack) path. (Bottom) ultrasonic signals propagated through damaged (simulated crack) path. Signals are presented for three stages of suborbital flight.

Fig. 19 illustrates signals corresponding to damaged (crack) and healthy (no crack) wave propagation paths that were collected during three stages of the suborbital spaceflight. The distinction between a path with a crack and without a crack is clear throughout all stages of the flight. For example, Fig. 19 shows the reduction in amplitude across the crack in sensor S5 record and the reflection from the crack in the sensor S1 signal at about 80 microseconds. The largest deviation within either damaged or healthy cases is again seen during the descent stage of the flight. These deviations are likely dominated by thermal processes.

II. CONCLUSIONS

In this contribution, results of ultrasonic measurements and wireless sensing during suborbital flight were reported. To our knowledge, no active pulse ultrasonic assessment experiments were done in space before and hence it is believed that the reported results may be of a considerable interest to researches working on SHM aspects for space vehicles.

Utility of wireless temperature and strain sensing during suborbital flight has been demonstrated. We are not aware of any prior application of wireless sensing to suborbital vehicles and the test was aimed at validating potential of wireless technology for suborbital flight. Experiments have demonstrated stable temperature and strain wireless data transfer during suborbital flight. Spatial distribution of temperature was noticed (as two nodes in the payload were employed) and strain signature representative of vehicle's dynamics was collected. It should be also mentioned that wireless technology was validated for compatibility with vehicle's systems and payloads and passed pre-launch qualifications. The successful test of wireless technology opens a wide array of opportunities for suborbital flight customers.

Ultrasonic hardware utilized in the tests allowed for passive recording of acoustic emission events. Although the hardware was not specifically designed for monitoring acoustic emission, it was decided to exercise such a measurement opportunity. The passive mode was able to record several of the rocket flight events including motor burn stage and payload separation stage. Therefore, the passive embedded ultrasonic mode can be valuable in monitoring the progress of a flight as well as recording events that may occur during re-entry of a space vehicle. Perhaps a dedicated hardware could be used to further improve acoustic emission monitoring at ultrasonic frequencies.

The active embedded ultrasonic mode was utilized to study elastic wave propagation in vehicle's structure during suborbital flight. Analysis of data from this mode initially suggested a permanent change in vehicle's structure reflected in the phase shift of elastic waves. Further investigations, which took the temperature effect into account, discovered that the phase shift was only temporary and dependent on the current system's temperature. However, even when comparing the ground operation and flight operations, and taking the temperature effect into account, there was a distinct amplitude reduction and phase shift in the anti-symmetric (A0) mode of the propagated pulse. This deviation cannot be attributed to temperature and is thought to be influenced by some other factor present during suborbital flight. The described effect should be considered for real-time diagnostics of space vehicles, particularly for techniques that utilize the anti-symmetric mode for SHM.

Structural bolted joints were monitored by active ultrasonics during suborbital flight. The data clearly allow for distinguishing healthy "tight" and damaged "loose" conditions of such joints. Comparison of ultrasonic records from intact and damaged (simulated crack) wavepaths suggests crack detection capability of embedded ultrasonics either in the through propagated ultrasonic pulse or in the crack-reflected pulse. Crack detection was confirmed during all stages of suborbital flight. Differences between records in similar groups (e.g. damaged or healthy) in both bolted joint or crack detection studies were rather small and were attributed to dominating contribution of thermal effects.

Unfortunately, the electromechanical impedance test did not yield useful data. It is believed that the reason for this was malfunctioning of the electronic equipment. Another failure on this flight was a GoPro® camera, which drained its batteries during several hours of the launch delay.

II. ACKNOWLEDGEMENTS

Authors would like to acknowledge the following contributors to the success of the program:

- The suborbital flight opportunity was provided by the NASA Flight Opportunities Program http://flightopportunities.nasa.gov , flight 38 BS.
- Federal Aviation Administration (FAA) through Center of Excellence for Commercial Space Transportation, AFRL Space Vehicles Directorate, and NMT Department of Mechanical Engineering are acknowledged for financial support.
- Los Alamos National Laboratory Engineering Institute for providing WID3 impedance measurements boards (Charles Farrar, Stuart Taylor, Gyuhae Park).
- Metis Design and LORD Microstrain for collaboration on measurement hardware and assistance with tests.
- Up Aerospace Corporation (Jerry Larson and the team) for successful payload integration, launch and recovery.

[1] Arritt, B.J., Robertson, L.M., Henderson, B.K., Ouyang, L., Beard, S., Clayton, E.H., Todd, M.D., Doyle, D., Zagrai, A., Buckley, S.J., Ganley, J.M., Welsh, J.S., (2008), "Structural Health Monitoring: an Enabler for Responsive Satellites," *Proceedings of SPIE*, Vol. 6935, 6935-38.

[2] Zagrai, A., Doyle, D., Gigineishvili, V., Brown, J., Gardenier, H., Arritt, B., (2010) "Piezoelectric Wafer Active Sensor Structural Health Monitoring of Space Structures," Journal of Intelligent Material Systems and Structures, Vol. 21, N. 9, pp. 921-940, first published on May 4, 2010.

[3] Sarafin T.P, and Doukas P.G, (2007), "Simplifying the Structural Verification Process to Accommodate Responsive Launch," *Proceedings of the 5th Responsive Space Conference*, AIAA-RC5 2007-5003.

[4] Ailor, W., (2011) Aerospace Corporation, personal communications.

[5] Ailor, W., Dupzyk, I., Shepard, J., Newfield, M., (2007) "REBR: An Innovative, Cost-Effective System for Return of Reentry Data," *Proceedings of AIAA Space 2007 Conference*

[6] Cuc, A., Giurgiutiu, V., Joshi, S., and Tidwell, Z., (2007), "Structural Health Monitoring with Piezoelectric Wafer Active Sensors for Space Applications," AIAA Journal, Vol. 45, No. 12, December, (2007).

[7] Mancini, S., Tumino, G., Gaudenzi, P., (2006), "Structural Health Monitoring for Future Space Vehicles," J. Intell. Mater. Syst. Struct, Vol. 17-July 2006, pp. 577-585.

[8] Kabashima, S., Ozaki, T., Takeda, N., (2001), "Structural health Monitoring using FBG Sensor in Space Environment," *Proceedings of SPIE*, Vol. 4332, pp. 78-87.

[9] Zagrai, A.N., Cooper, B., Schlavin, J., White, C., and Kessler S., (2013) "Structural Health Monitoring in Near-Space Environment, a High Altitude Balloon Test," *Proceedings of 9th International Workshop of Structural Health Monitoring*, 10-12 September 2013, Stanford University, California, pp. 1840-1847.

[10] Park, G., Sohn, H., Farrar, C.R., and Inman, D. (2003) "Overview of Piezoelectric Impedance-Based Health Monitoring and Path Forward," The Shock and Vibration Digest, 2003, Vol. 35, N. 6, pp. 451-463.

[11] Park, G., Cudney, H.H., and Inman D.J. (2001) "An Integrated Health Monitoring Technique Using Structural Impedance Sensors," Journal of Intelligent Material Systems and Structures, Vol. 11, pp. 448-455.

[12] Giurgiutiu, V., Reynolds, A., and Rogers, C.A. (1999) "Experimental Investigation of E/M Impedance Health Monitoring of Spot-Welded Structural Joints," Journal of Intelligent Material Systems and Structures, Vol. 10, October – 1999, pp. 802-812.

[13] Liang, C., Sun, F. P., and Rogers C. A., (1993), "An Impedance Method for Dynamic Analysis of Active Material Systems," Proceedings, 34th AIAA/ASME/ASCE/AHS/ASC SDM Conference, pp. 3587-3599.

[14] Giurgiutiu, V. and Rogers, C.A., (1997), ''Electro-Mechanical (E/M) Impedance Method for Structural Health Monitoring and Non-Destructive Evaluation,'' Int. Workshop on Structural Health Monitoring, Stanford University, CA, Sep. 18–20, pp. 433–444.

[15] Shull, P.J., (2002) *Nondestructive Evaluation: Theory, Techniques, and Applications*, CRC Press.

[16] Guirgiutiu, V., (2014) *Structural Health Monitoring with Piezoelectric Wafer Active Sensors*, Academic Press.

[17] Mascarenas, D.L., Todd, M.D., Park, G., Farrar, C.R., (2006) "A Miniaturized Electromechanical Impedance-based Node for the Wireless Interrogation of Structural Health," *Proceedings of SPIE on Health Monitoring and Smart Nondestructive Evaluation of Structural and Biological Systems V*, Vol. 6177, 61770T.